Zinc-Substituted Hemoglobins: α- and β-Chain Differences Monitored by High-Resolution Emission Spectroscopy†

Katakam Sudhakar,‡ Monique Laberge, Antonio Tsuneshige, and Jane M. Vanderkooi*

Johnson Research Foundation, Department of Biochemistry and Biophysics, School of Medicine, University of Pennsylvania, Philadelphia, Pennsylvania 19104

Received November 12, 1997; Revised Manuscript Received February 10, 1998

ABSTRACT: The absorption and emission properties of hybrid Zn-substituted human hemoglobin (Hb) were used to monitor differences in interaction between the porphyrin and the polypeptide chain for the two subunits. Although α-substituted (α-ZnHb), β-substituted (β-ZnHb), or totally substituted Hb all show optical properties characteristic of Zn porphyrins, the spectra are also indicative of specific interactions between the polypeptide chain and the porphyrin. The $Q_{0,0}$ absorption band of α-ZnHb at 5 K shows a splitting of ∼300 cm^{-1}, comparable to the largest split ever reported for a heme protein. This value is ∼140 cm^{-1} for β-ZnHb. The possible origin of the split is discussed in terms of the local electric field imposed by the amino acids of the respective heme pockets, different configurations of the porphyrin, and/or influences of the liganding histidine. The Zn derivatives show quasiline spectra under fluorescence line narrowing conditions, and the resolved excitation spectrum reveals differences in the vibrational levels of the Zn porphyrin in the two subunits. Broad underlying emission in the fluorescence line-narrowed emission spectrum can be accounted for, in part, by the existence of the two closely spaced electronic origins and also by the extent of phonon coupling between the porphyrin and the protein matrix.

When O_2 binds to the iron of one of the hemoglobin (Hb)[1] subunits, there is a conformational change that alters the binding affinity of O_2 to the heme in contiguous subunits. This conformational transition remains one of the most intensively investigated phenomena in structural biology and has become a paradigm for the study of information transfer from one part of a protein to another. A great deal of data is available on how ligation—with its associated changes in bond lengths and angles—produces a conformational change throughout the $\alpha_2\beta_2$ heterotetramer. Less information, however, is available on how conformational changes occurring in one subunit ultimately affect the electronic properties of the heme in a neighboring subunit. Indeed, one of the interesting remaining problems is why there are two subunits, the α and the β. Both are needed, as shown by the observation that, in cases where the ratio of α and β subunits is impaired, the disease thalassemia results (*1*).

To study the functional differences between the two subunits, we have started using hybrid derivatives of Hb in which we substitute zinc for the native iron in one or both Hb subunits. Since Zn is a closed-shell metal, it does not bind oxygen, and any effect of the polypeptide chain on the spectrum is thus independent of the spin state of the central metal and can then be attributed to heme pocket interaction with the porphyrin. Hybrid derivatives have been long used to examine subunit interactions (*2*−*4*). The fluorescence and phosphorescence quantum yield of the Zn porphyrin in Hb is high, and therefore, emission is easily detectable (*3*). Unlike hemes, the excited-state lifetimes of Zn porphyrins are long, and consequently, excited-state reactions can be monitored. For example, hybrid met Hbs Zn_2Fe_2Hb and Mg_2Fe_2 Hb have been used to study light-induced electron transfer (*5*−*7*).

In this paper, we are primarily focusing on the electronic spectral properties of the ZnHb derivatives, using high-resolution optical spectroscopy. We show that the heme environment in both subunits induces enough asymmetry in the porphyrin so as to split the $Q_{0,0}$ absorption and that the split is greater in the α subunit. Under fluorescence line narrowing (FLN) conditions, i.e., low temperature and narrow band excitation, Zn porphyrins in proteins exhibit sharp emission lines called the zero phonon lines (ZPL) (*8*−*10*). The ZPL allow us to determine the extent of the inhomogeneous broadening of the electronic transition and allow for construction of vibrationally resolved excitation spectra. These data yield information on the phonon coupling and the configuration of the porphyrin, respectively.

MATERIALS AND METHODS

Preparation of Hybrid Hemoglobins. Zn hemoglobin derivatives were prepared from human hemoglobin as previously described (*11*). Water was deionized and glass distilled. Other chemicals were of the highest purity commercially obtainable.

Oxygen Removal from Samples. The samples were first degassed by aspiration, and the air space in the sample tube was filled with argon. A small volume of solution containing

† Supported by Division of General Medicine of the National Institutes of Health Grant PO1 GM48130.

* To whom correspondence should be addressed. Fax: 215-573-2042. E-mail: vanderko@mail.med.upenn.edu.

‡ Present address: SAIC Frederick, Bldg 535 Room 424, NCI−FCRDC, Frederick, MD 21702.

[1] Abbreviations: Hb, hemoglobin; α-ZnHb, $\alpha(Zn)_2\,\beta(Fe)_2$Hb; β-ZnHb, $\alpha(Fe)_2\,\beta(Zn)_2$Hb; ZnHb, $\alpha(Zn)_2\,\beta(Zn)_2$Hb; IDF, inhomogeneous distribution function; FLN, fluorescence line narrowing; BTP, bis-tris propane; ZPL, zero phonon line.

S0006-2960(97)02786-4 CCC: $15.00
Published on Web 05/02/1998

glucose, glucose oxidase, and catalase was then added to give final concentrations of 10 mM, 80 nM, and 16 nM, respectively. These enzymes catalyze the reduction of O_2 to H_2O_2 and then to H_2O by glucose. The sample tube was then closed with a lid and sealed with Parafilm.

Instrumentation. Conventional absorption spectra were recorded on a Hitachi U-3000 UV−vis spectrophotometer. This instrument was calibrated with the deuterium lamp emission line and is accurate ±0.3 nm. The spectra were acquired at a 0.5 nm resolution. For absorption measurements at 4.2 K, a closed cycle CF1204 Cryostat (Oxford Instruments, England) was used.

Fluorescence and phosphorescence emission spectra were obtained using a Perkin-Elmer LS5 luminescence spectrometer. For measurements at 77 K, a coldfinger liquid nitrogen Dewar was used. The FLN spectra were acquired as described previously (*4*). The sample was cooled in an open cycle EPR Cryostat (Air Products, Allentown, PA). The laser excitation light was defocused so as to minimize hole burning effects.

Data Analysis: Energy Inhomogeneous Distribution Function (IDF) and Vibrationally Resolved Excitation Spectrum. For long-lived excited-state molecules, excitation into a vibronic band is followed by relaxation to the lowest electronic level of the excited state. Personov and coworkers have shown that, in the case of aromatic molecules—such as porphyrins—which have inhomogeneously broadened spectra, a single excitation frequency can excite multiple vibrational levels (*12, 13*). Multiple 0,0 emission lines are then observed, separated by the vibrational frequencies of the excited-state molecule. By plotting the intensity of a given vibrational line as one varies the excitation frequency, a curve can be obtained representing the inhomogeneity of the electronic transition energy (*14, 15*). This plot is referred to as the inhomogeneous distribution function (IDF). As such, it represents the true electronic transition, extracted from the homogeneous broadened background.

The near equivalent of a vibrationally resolved excitation spectrum was obtained from the spectra used to obtain the IDF by summing the emission spectra in the 0,0 region when their abscissa are expressed as a difference from excitation (*16*).

Electrostatics. The X-ray structure of human deoxyhemoglobin (*17*) was used to extract α-Hb and β-Hb heme environments with the *InsightII* software package (MSI, San Diego). A sphere extending to 14 Å from each heme was extracted from the X-ray structure from the α1 and β1 subunits to show representative heme environments. The potentials were calculated at each heme (43 atoms) using the GRASP program as previously described (*18*) and used (*19, 20*). The electrostatic parameters were dielectric constants of 80 and 2 for protein and solvent, respectively, 1.4 Å probe radius, 0.01 μ ionic strength. The potentials were calculated at all vertexes and atoms of the heme with the protein charged using parse3 charges (*21*).

RESULTS

Absorption and Emission at Room Temperature. The visible absorption and fluorescence spectra of the Zn-substituted hemoglobins are shown in Figure 1. At room temperature, the spectra exhibit typical closed-shell metal porphyrin characteristics: two absorption maxima, the $Q_{0,0}$—or α band—at lower frequency and the $Q_{0,1}$—or β band—at higher frequency, the latter consisting of many vibronic bands (*22*). The $Q_{0,0}$ absorption band of the α-substituted Hb (α-ZnHb) is relatively broader at room temperature than that observed for the protein with Zn substituted in the β-chain (β-ZnHb). It should be noted that the absorption spectra of the hybrid derivatives also contain contributions from the unsubstituted heme. This is apparent in the increased absorption at ~19 000 cm^{-1} in the mixed hybrids (top, middle) when compared to the totally Zn-substituted protein (bottom). The fluorescence is characterized by a Stokes shifted $Q_{0,0}$ band and an approximate mirror image $Q_{0,1}$ band emission at lower frequency. The emission spectra were independent of exciting wavelength: no detectable difference was observed when the excitation was either at 400 nm or in the $Q_{0,1}$ region. Table 1 summarizes the conventional absorption and emission characteristics of the Zn hybrid hemoglobins, as well as the phosphorescence emission and lifetime data. As with fluorescence, the emission maximum of the α-ZnHb phosphorescence is at lower frequency than that of β-ZnHb. At 300 K, the fully Zn-substituted hemoglobin has an emission maximum that is the approximate mean of the two individual subunits. Since the emission maxima of the α and β units are close and the bands wide, the sum of these emissions thus yields the fully substituted spectral emission envelope. It is also well-known that there are small but real differences in the optical

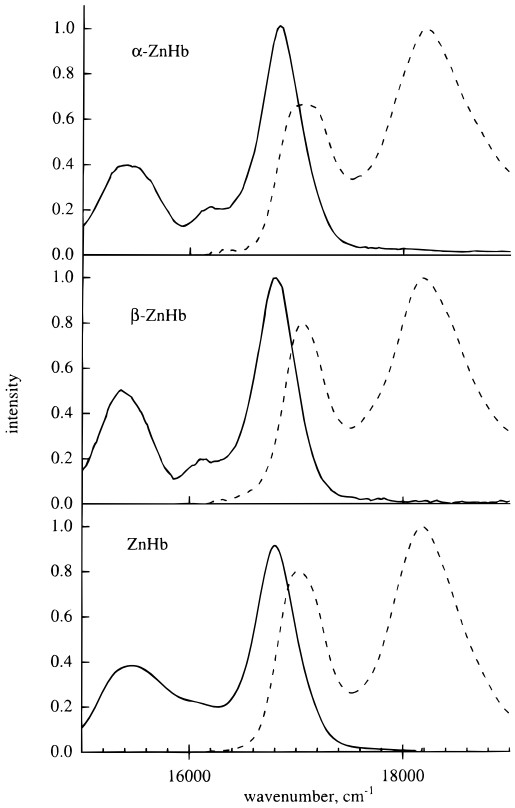

FIGURE 1: Absorption (dotted line) and emission (solid line, arbitrary units) spectra of ZnHb derivatives at 20 °C. The sample was ~1 μM in 0.1 M BTP buffer and 0.1 M NaCl at pH 6.0. Excitation was at 400 nm; spectral band-pass was 5 nm. Deoxygenation was achieved by adding sodium dithionate solution to the sample. (Top) α-ZnHb; (middle) β-ZnHb; (bottom) ZnHb.

Table 1: Absorption and Emission Properties of Zn-Substituted Hb

	α-ZnHb	β-ZnHb	ZnHb	temp, K
absorption/fluorescence				
$Q_{0,0}$ absorption max, cm^{-1}	~17 000 (broad)	~17 007	~17 000	300
$Q_{0,0}$ emission max, cm^{-1}	~16 830	~16 800	~17 650	300
$Q_{0,0}$ absorption max, cm^{-1}	~16 998, 17301	17 068, 17 209		5
IDF maximum, cm^{-1}	16 900	17 000		5
IDF width, cm^{-1}, fwhm	~140	~100, shoulder		5
phosphorescence				
emission max, cm^{-1} (nm)	13 830 (723)	13 910 (719)	13 870 (721)	77
lifetime, msec	29	29	31	77

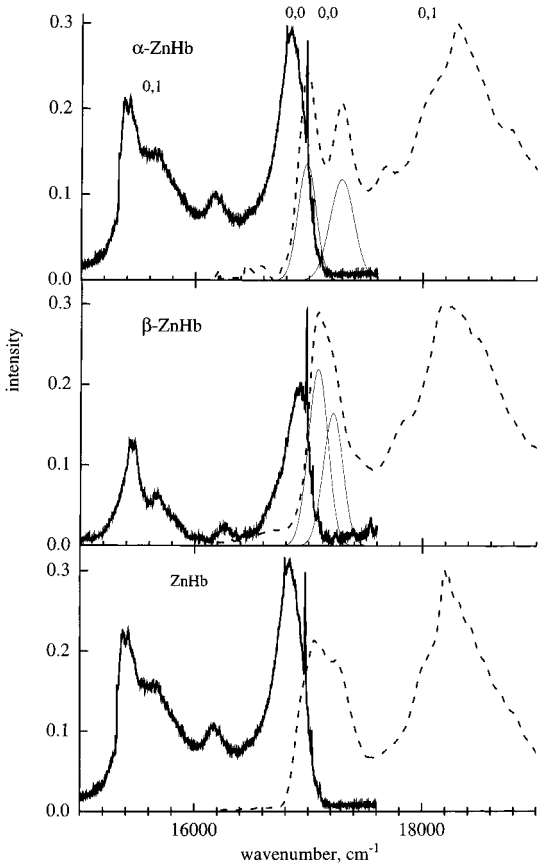

FIGURE 2: Absorption (dotted line) and emission (solid line, arbitrary units) spectra of α-ZnHb at 5 K. The sample was 200 μM protein in 50% glycerol and 50% buffer (0.1 M BTP and 0.1 M NaCl, pH 6.0). Absorption was recorded with a UV−vis spectrophotometer and the emission spectra are selectively laser-excited at 17700 cm^{-1}. (Top) α-ZnHb; (middle) β-ZnHb; (bottom) ZnHb. Hairline curves: Gaussian fits centered at 16 998 and 17 301 cm^{-1} for α-ZnHb and at 10 068 and 17 209 cm^{-1} for β-ZnHb.

absorption spectra of the hemes in the two subunits of Hb (*23*).

Low-Temperature Absorption and Emission. Additional features are obtained in the absorption and emission spectra when the samples are cooled to 5 K (Figure 2). In the case of α-ZnHb, a most striking spectral feature is the observed $Q_{0,0}$ band splitting in absorption. The peak maxima are at 16 998 and 17 301 cm^{-1}, corresponding to a spectral splitting of 303 cm^{-1}. The absorption in the $Q_{0,1}$ region begins to show unresolved vibronic resolution. The FLN emission is more resolved —due to selective laser excitation—and shows narrow ZPL features, especially in the $Q_{0,0}$ region, which are superposed on broader features.

The absorption and emission spectra of β-ZnHb at 5 K are also shown in Figure 2 (middle). The $Q_{0,0}$ absorption band is asymmetric, and a Gaussian deconvolution procedure yields two maxima centered at 17 068 and 17 209 cm^{-1}, corresponding to a spectral splitting of 141 cm^{-1}. As noted above, at room temperature, the spectrum of β-ZnHb shows a narrower $Q_{0,0}$ absorption band than the spectrum of α-ZnHb (Figure 1). This suggests that, at that temperature, the relatively larger split in the absorption band of the α-ZnHb accounts for its broader absorption. The β-Zn derivative also shows resolved emission.

The absorption peaks for ZnHb are approximately the summed average of the two spectra of the substituted subunits (Figure 2, bottom) minus the broad absorbance due to the two deoxy-Fe heme subunits also present in the hybrid Hbs. The fluorescence emission spectrum is also approximately the sum of the individual Zn components (since Fe hemes do not fluoresce).

FLN Spectroscopy: Determination of the Origin Frequency and Vibrational Levels of the Excited State. Figure 3 compares the sharp features in the FLN spectra of the Zn hybrids obtained in the $Q_{0,0}$ region as a function of excitation frequency into the $Q_{0,1}$ region. The vibronic bands are highly resolved and clearly distinguishable from the broad background.

The IDFs of α-ZnHb and β-ZnHb are also plotted in Figure 3 at the top of the respective FLN spectra. The maxima of the two IDFs and the approximate widths are given in Table 1. In the case of α-ZnHb, the IDF has a single major maximum, although the distribution was not strictly Gaussian. We conclude that there is one major population—and hence also one mean conformation—which has a distribution of energy in its electronic transitions. Even at 5 K, the absorption and emission of the origin do not exactly coincide, and the IDF, which represents the distribution of the real electronic origin, lies between the two. The IDF of β-ZnHb is not so clear-cut, and it is difficult to evaluate whether we are seeing a bimodal distribution or a single maximum with pronounced data scatter at lower energy. In the previous FLN study in this series, i.e., that of the iron-free Hb hybrids (*4*), the β-iron-free hybrid clearly showed a bimodal distribution, and it was speculated that this could be indicative of two β-Hb protein conformations. Clearly, more data is required to address this point fully in the case of the Zn hybrids.

As explained above, we summed the series of emission spectra shown in Figure 3, and we acquired spectra at different excitation wavelengths to construct the equivalent of a vibrationally resolved excitation spectrum. These are shown in Figure 4. The frequencies of the ZPLs are given in Table 2. We see that the α and β spectra differ in their vibrational frequencies (cf. Figure 4 and Table 2). For instance, in the region of the spectrum between 600 and 650

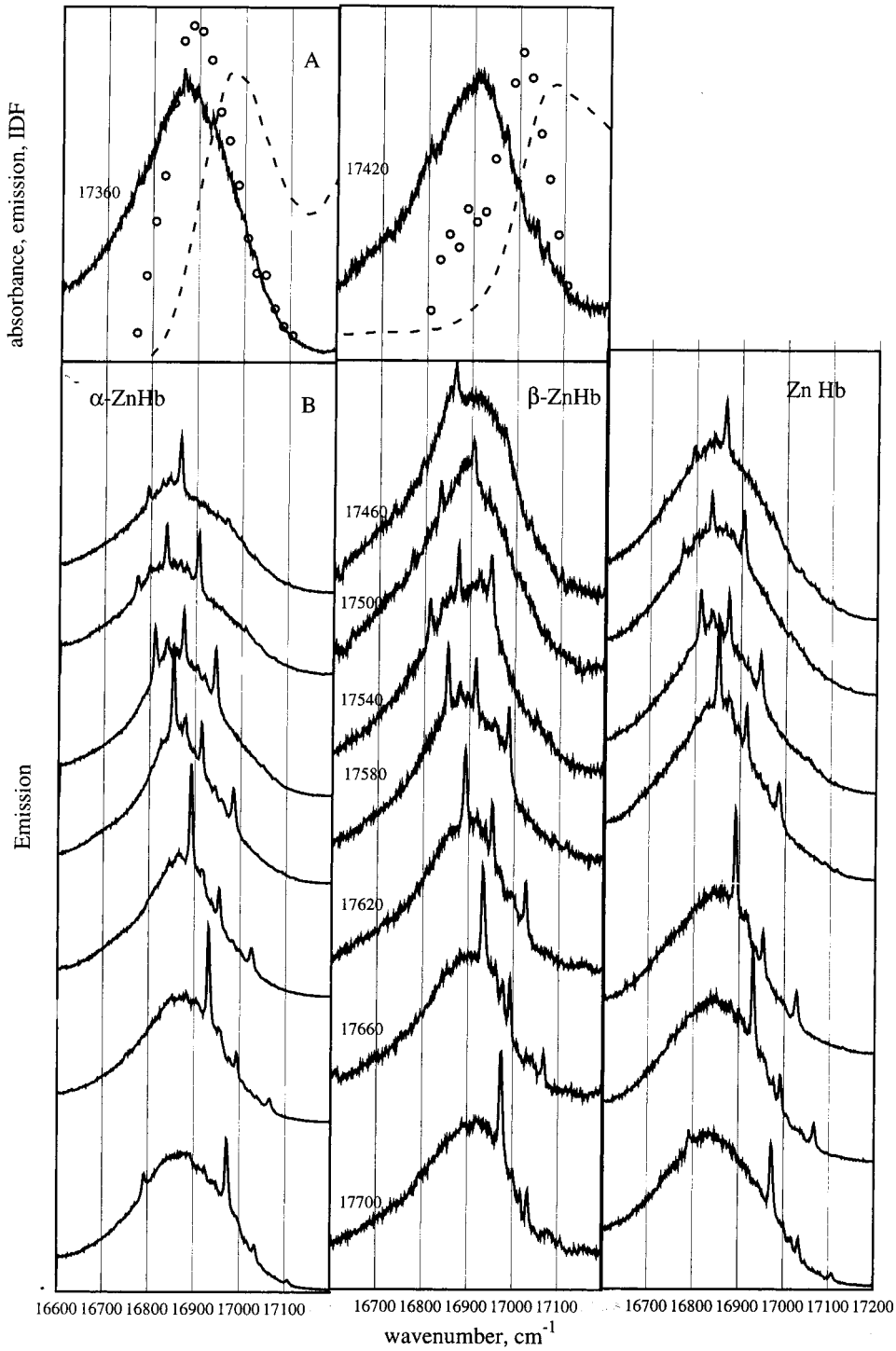

FIGURE 3: FLN spectra of the Zn-hybrids acquired in the $Q_{0,0}$ region. The concentration of protein was 200 μM in 50% glycerol and 50% 0.1 M BTP buffer at pH 6.0. Temperature maintained at 5 K. (A) IDF (○), absorption (dotted line) and emission spectra (solid line) at excitation indicated. (B) FLN spectra the 0,0 region as a function of excitation frequency, indicated on the Figure. (Left) α-ZnHb; (middle) β-ZnHb; (right) fully substituted ZnHb.

cm^{-1}, the α spectrum shows two vibrations at 621 and 637 cm^{-1} while the β spectrum only shows one (617 cm^{-1}).

Temperature Dependence. FLN spectra are best observed when the phonon coupling is relatively weak (*13*) and when the energy selection is retained in the excited state, i.e., where excited-state reactions do not occur. The temperature dependence of the FLN spectra is shown in Figure 5 for both α-ZnHb and β-ZnHb. At about 40 K, resolution disappears and both Zn derivatives show a very similar temperature dependence.

DISCUSSION

The function of the α and β subunits is essentially the same: to bind and release oxygen. While the overall folding of the polypeptide chain is very similar, less than 50% percent of the sequence is conserved in the α and β subunits. Some flexibility in the protein matrix is required to allow diffusion of O_2 through the protein and binding to the heme; in addition, the polypeptide chain has to modulate the chemistry of the heme so that oxygen binds while the iron

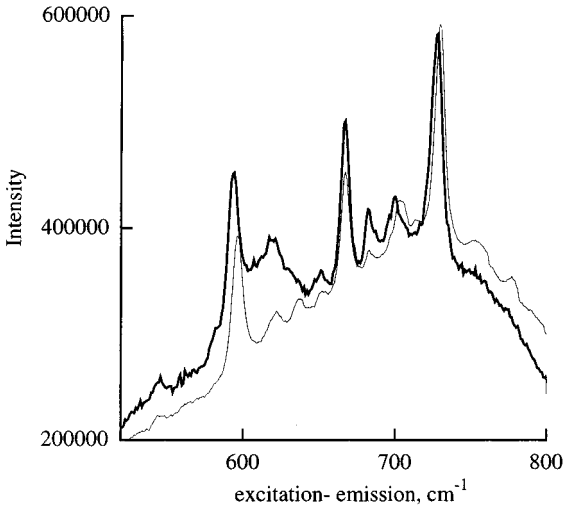

FIGURE 4: Vibrationally resolved excitation spectra. Emission spectra taken at 20 cm^{-1} increments from 17 360 to 17 700 cm^{-1} in excitation were converted to frequency difference from excitation and then summed. (Hairline) α-ZnHb. (Bold) β-ZnHb. Conditions given in Figure 3.

Table 2: Vibrational Line Frequencies, cm^{-1}, from Excitation[a]

α-ZnHb	β-ZnHb
596 s	594 s
621 w	617 b
637 w	
651 w	651 w
667 s	667 s
682 w	682 w
698 w	700 w
729 s	727 s

[a] s, strong; w, weak; b, broad.

remains reduced. How the *different* amino acids modulate the oxygen binding environments (i.e., the hemes) that perform very much the *same* function is an interesting question.

High-resolution optical spectroscopy provides a means to examine the influence of the environment on the porphyrin. In FLN, a narrow band laser is used to excite the sample which is held at low temperature (*13*). The narrow band selectively excites one subpopulation among the population of molecules with inhomogeneously distributed electronic transitions. Among the information that can be obtained are vibrationally resolved spectra of both ground and excited states, electron−phonon coupling approximations and the distribution of 0,0 energies (*10*). These spectral parameters can then be used to examine the differences between the two subunits.

Spectral Splitting. The splitting observed in the $Q_{0,0}$ band absorption region is most interesting. The splitting is much larger for Zn porphyrin in the α chain (303 cm^{-1}) than that observed in the β chain (cf. 141 cm^{-1}).

Splitting of the $Q_{0,0}$ band of ferrous heme proteins and metalloporphyrins at cryogenic temperatures was originally observed by Keilin (*24*), and there are many examples found in the literature (see references in ref *25*). An explanation for the split is that the asymmetry of the heme environment distorts the porphyrin so that it lifts the strict D_{4h} symmetry (*25*, *26*). Theoretical considerations would predict that the absorption should be greater for the lower energy band (*27*), and this was indeed observed (cf. Figure 2). Jahn−Teller

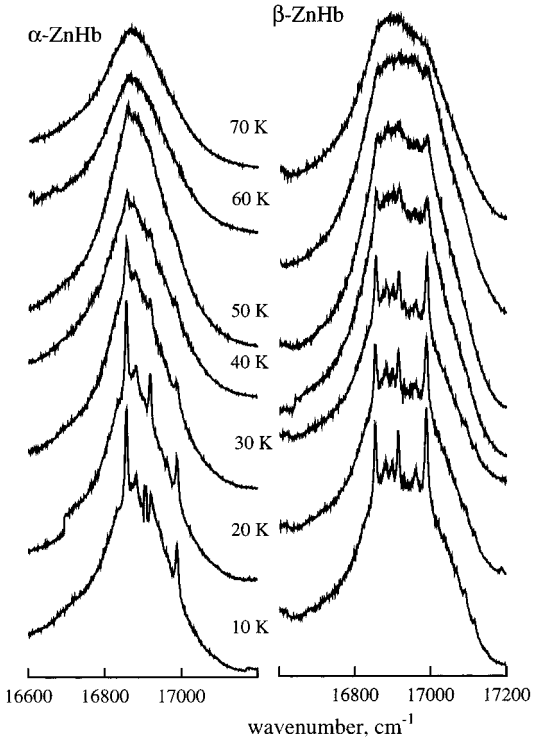

FIGURE 5: Effect of temperature on the emission spectrum. The concentration of α-ZnHb was 200 μM in 50% glycerol and 50% 0.1 M BTP buffer at pH 6.0. Temperatures are indicated on the figure. Excitation: 17 580 cm^{-1}. (Left) α-ZnHb; (right) β-ZnHb.

instability of triplet state metalloporphyrins is well documented (*28*, *29*) and has been proposed for porphyrins in hemoglobin (*30*−*32*) and other heme proteins as well (*33*). How triplet state configurations relate to singlet state configurations, however, remains an open question.

Assuming that the electronic spectrum is split into two closely lying electronic levels, we can interpret some features of the observed fluorescence. When excitation is into the higher electronic manifold, nonresolved emission should be expected, for several reasons: (i) The population of molecules is likely to have a distribution in the splitting energy for the two electronic levels. In this case, excitation on the higher energy side of the higher energy band would lead to emission on the lower energy side of the lower energy band (whereas excitation on the lower energy side would give emission on the higher energy side). Under these conditions, energy selection would be lost. The possibility that there is a distribution of Jahn−Teller split energy in case of Zn-porphyrin triplet state of cytochrome *c* derivatives is supported by electron paramagnetic resonance (*33*). This is unlike the case when excitation is into a higher vibronic level of the *lower* electronic manifold. It has been shown that, in this case, although the electronic level is inhomogeneously distributed, the vibrational levels are approximately constant (*13*). (ii) Transfer from one electronic surface to another would involve coupling with the phonon wings, and energy selection would not be maintained. For example, excitation into the S_1 level with subsequent intersystem crossing to the triplet state does not yield resolved phosphorescence spectra in these porphyrin-protein systems. (iii) Excitation into another electronic manifold could yield unresolved emission because relaxation from this excited state to the lower electronic manifold is likely to be very fast (*34*), and hence, the emission lines would be broad.

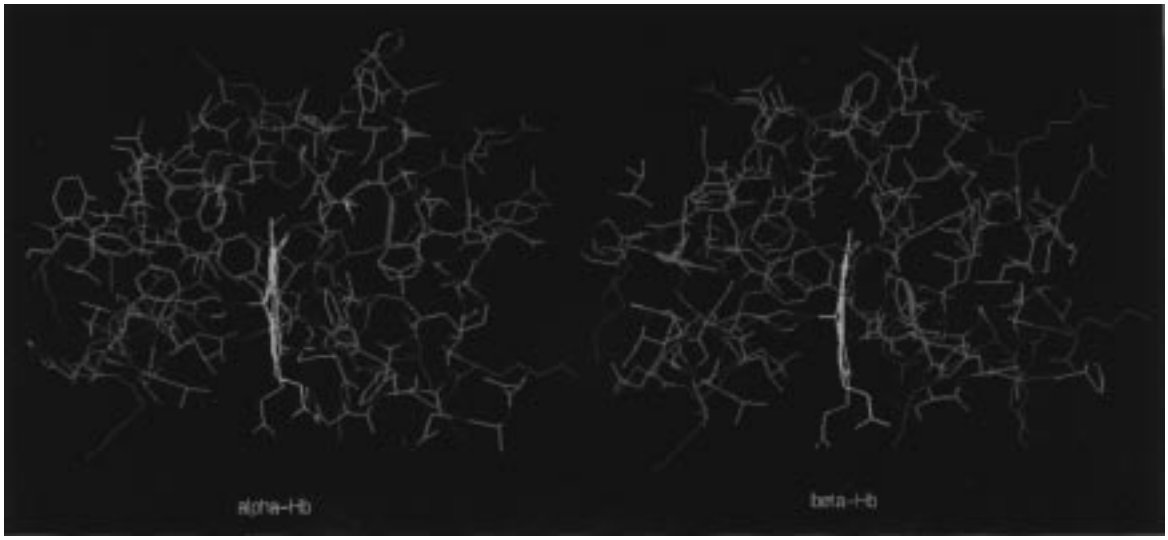

FIGURE 6: Distribution of charged residues in α-Hb and *β*-Hb within a 14 Å sphere around the heme extracted from the 1.7 Å X-ray structure (pdb2hhb.ent, Brookhaven Protein Data Bank) (*49*). The negatively charged residues (glu, asp) are red and the positively charged (lys, arg) are blue.

We therefore expect that excitation into the vibronic bands of the lower electronic manifold—but not exciting into the higher electronic level—would lead to resolved emission. There is no duplication of the sharp emission features in the spectra (Figure 2). This has also been observed in the case of crystalline porphyrins (*35*). The loss of degeneracy resulting in split electronic levels could explain why the emission from the ZnHb derivatives shows larger "background" fluorescence than do the metal-free Hb derivatives (cf. Figures 2 and 3 in ref *4* with Figure 2). Two closely associated electronic levels in Zn porphyrins could also account for the greater unstructured background observed in the case of Zn cytochrome *c* than for iron-free cytochrome *c* (*36*−*38*).

In our context, the question of interest then becomes what in the environment of the heme pocket could possibly promote such large $Q_{0,0}$ splitting? From symmetry considerations, distortions of the respective porphyrin planarities could conceivably cause splitting. The FLN spectra of Figure 2 were obtained by exciting into a higher vibronic line, resulting in the observation of multiple 0,0 lines. As such, these lines provide vibrational details on the excited-state molecule. The vibrational frequencies are different for the two Zn Hb derivatives between 600 and 650 cm^{-1} (cf. Table 2). This is the region of porphyrin resonance Raman pyrrole deformation modes (e.g., $\delta_{pyrr.def.sym}$ at 605 cm^{-1} in Nickel octaethylporphine) (*39, 40*) and out-of-plane modes for cytochrome *c* (e.g., pyrrole swivel at 612 cm^{-1}) (*41*). The purpose here is not make decisive vibrational assignments but to point out that there are vibrational spectral differences in the respective FLN spectra of both ZnHb derivatives that are observed in the region most sensitive to the type of porphyrin distortion most likely to result in that specific porphyrin asymmetry required to lift—or at least—affect the D_{4h} degeneracy. Differences in the heme configuration in the α- and *β*-subunits have also been monitored by resonance Raman on a cobalt Hb derivative (*42*).

The orientation of the histidine ligand relative to the heme plane may also be significant in altering the electronic splitting. The splitting in the α-ZnHb is comparable to ∼300 cm^{-1} found in the Mg and Zn derivatives of sperm whale myoglobin (*43, 44*). In Mb, the His ligand is almost oriented over a straight line connecting two opposing pyrrole nitrogens. However, this is not the case in either subunit of Hb. From this, we conclude that the orientation of the His ligand cannot be a factor in causing the observed splittings. However, the α and *β* hemes do have slightly different geometries. In the α-hemes, the normals to the mean pyrrole planes are uniformly tilted toward the center of the porphyrin by ∼3° relative to the heme normal and the heme folds by ∼4° about an axis along the methene carbons located between the pyrrole rings that have similar substituents. The *β*-hemes show no such folding and two of their pyrroles are more tilted than that of the α-hemes by ∼8° (*17*). These considerations could argue for the involvement of some degree of porphyrin distortion in the Q-band splitting. The orientation may be different in the metal-substituted protein, the structure of which is not known; however, Zn porphyrins tend to be five liganded (*45*), even in cytochrome *c* where Zn derivative has the overall folding as the native Fe protein (*46*). This would argue that Zn Hb is a good model for the T state.

Another cause to be considered for the observed splitting is the local electric field produced by the amino acids surrounding the heme, with a significant contribution from electrostatic charge−charge interactions arising from adjacent charged amino acids, as presently investigated in a separate study. Recent Stark effect hole burning experiments and electrostatic field calculations on a c-type cytochrome have showed that different heme geometries could be distinguished through their behavior in an external field (*20*), and the vibrational spectra of small cytochrome *c* ligands can be shifted by modification of the protein matrix electrostatic field (*21, 47*). Figure 6 illustrates the distribution of charged residues liable to result in a spectrally significant Stark-type of splitting (red residues, negatively charged at pH 7, and blue residues, positive). It can be seen that, within a radius of overall net electrostatic influence (14 Å), the matrix distribution of charged residues responsible for charge−charge interactions differs significantly in both heme evironments. For example,compare the top left upper region in both subunits: α-Hb shows a distinct positive region,

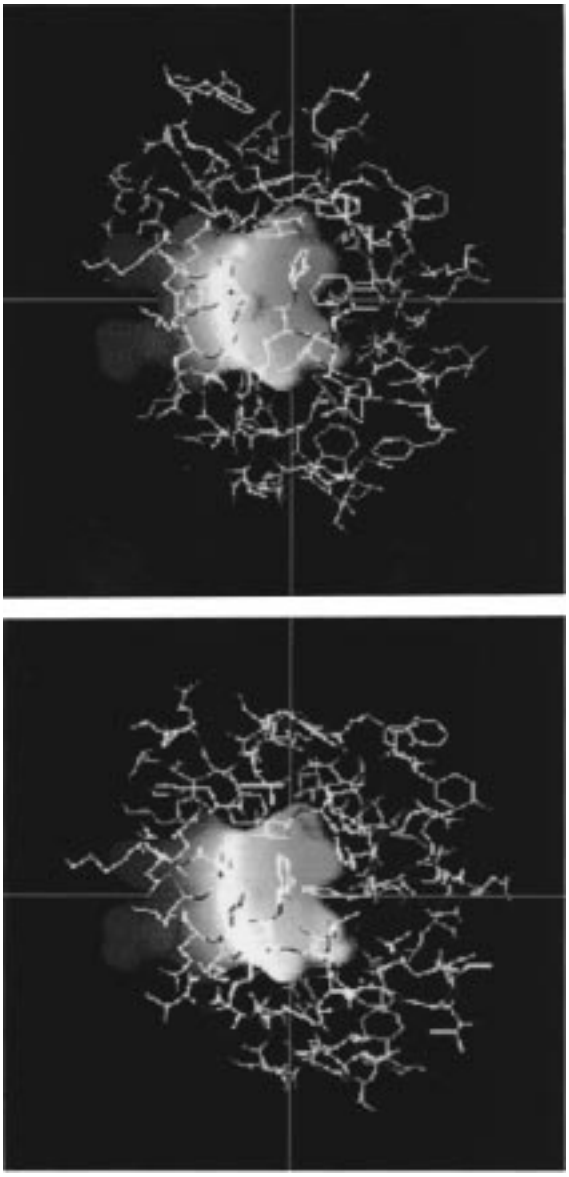

FIGURE 7: Electrostatic surface potential maps of the hemes in α-Hb (top) and *β*-Hb (bottom) using Hb subset-spheres including all residues within 14 Å of the respective Fe atoms. The protein matrix was charged using the parse3 charge parameters, the protein dielectric was 80 and that of the solvent 2. Calculations were performed using GRASP. The heme surface is color-coded according to its electrostatic potential: red = minimum values (negative); white = neutral potential region; blue = maximum values (positive).

while *β*-Hb has overlapping negative residues. Also, differences can be observed to the right side of the respective heme. Figure 7 presents electrostatic potential maps for both α- and *β*-heme environments. The results are preliminary in that other interactions besides the monopole−monopole can potentially contribute to spectral Stark shifts, but one trend emerges clearly, which is that the surface region of negative potential in the *β*-heme (red ≈ −320 mV) is less pronounced than that of the α-Hb, which is thus more negative (red ≈ −346 mV). These potential maps by no means represent a complete electrostatics study but they do point to a calculated difference in the monopole−monopole contribution to the surface potential. Further analysis should allow us to state if the magnitude of the split is consistent with the calculated electrostatic differences.

Finally, longer range effects could also be considered as contributing to the observed splitting. Heme−heme excitonic coupling has been suggested for Soret circular dichroism spectra for hemoglobin (*48*). Interaction between the Zn porphyrin and the heme of the neighboring subunit can be inferred from the shorter phosphorescence lifetime recorded for the mixed hybrid than for the totally Zn-substituted protein (Table 1). But we do not believe that such long-range interactions are playing a significant role in the spectral splitting. Energy transfer, resulting in quenching of phosphorescence, would be a longer range process than a direct excitonic process, which could also cause spectral modifications. Moreover, the totally Zn-substituted Hb exhibited spectral properties that were approximately the average of the individual Zn-subunit spectra (Table 1); this argues against excitonic coupling, since such a process would be different for the Zn and Fe porphyrins. Additionally, since metal-substituted Mb also shows a splitting comparable to that of α-ZnHb, excitonic coupling is then definitely not required to account for such splitting.

Stokes Shift, IDF, Phonon Coupling. In the absence of all interactions with solvent, the electronic absorption and emission origins should coincide. A Stokes shift at room temperature (Table 1) is indicative of the occurrence of relaxation processes.

Even at 5 K, the absorption and emission bands do not coincide (Figure 2). The IDF yields a value intermediate to the maxima directly observed in the spectra. The phonon wings associated with a ZPL are to higher energy in absorption and to lower energy in emission (*49*). We take the lack of coincidence to indicate that electronic transition of the porphyrin is affected by phonon coupling to the protein matrix.

Since the IDF is obtained from the ZPL, it gives the true distribution of 0,0 energies, undistorted from phonon contributions. For α-ZnHb, the maximum of the IDF is at 16 900 cm^{-1}; for *β*-ZnHb the value is at 17 000 cm^{-1} if the distribution is not bimodal. The splitting of the $Q_{0,0}$ transition is ∼303 and 141 cm^{-1}, respectively, and therefore, the transition energies in the absence of splitting would be at 17 050 cm^{-1} for α-ZnHb and 17 070 cm^{-1} for *β*-ZnHb. The absorption transition frequency in the absence of splitting can be derived by taking the average of the position of the two bands. For α-ZnHb it would occur at 17 149 cm^{-1} (average of 17 301 and 16 998 cm^{-1}) and for *β*-ZnHb at 17 137 cm^{-1} (average of 17 068 and 17 209 cm^{-1}). Therefore, for both the IDF and the absorption, within error, the largest effect of the protein matrix is on the splitting of the transition, with very little effect on the absolute energy of the origin.

For the Zn Hb derivatives, the IDF and the extent of phonon coupling can be compared to that of Mg-substituted horseradish peroxidase, which was subjected to a similar FLN study. In this case, there was a close correspondence between the absorption, emission, and IDF (*26*). This suggests that, in the hemoglobin, the porphyrin is more tightly coupled with the polypeptide chain relative to the peroxidase protein, producing a larger phonon wing contribution.

Temperature Dependence. The temperature dependence of the FLN spectra was remarkably similar for both derivatives, with disappearance of resolution above ∼40 K. The

processes discussed above, such as phonon coupling and relaxation between electronic levels are temperature dependent and they usually result in loss of spectral resolution. The temperature dependence is unlikely to be related to thermal equilibration of the electronic levels since the observed Q-band splittings are different for the two derivatives, but temperature dependence is similar. Furthermore, because of the large splitting, we would expect thermal equilibrium between the two electronic forms only to occur at higher temperatures. Another cause for loss of energy selection conditions could be due to the neighboring atoms changing position during the absorption and emission processes. This would shift the emission spectrum randomly and result in broadening. It is known that CO upon photodissociation can reversibly bind Hb above 20 K (*50*) showing that there is motion in the atoms sufficient to allow the diffusion of CO. Therefore, it is likely that the spectral changes observed during the temperature dependence is a type of glass transition, where motion of some residues begins to occur, sufficient to cause loss of resolution in the spectra.

In summary, the Zn derivatives of hemoglobin reveal interactions between the polypeptide chain and the porphyrin. We suggest that there is asymmetry in the heme pocket that reduces the symmetry of the heme. This is most pronounced in the α-subunit, leading to one of the largest split in the $Q_{0,0}$ absorption band so far observed in heme proteins. Other spectral features of the Zn porphyrin in the two subunits were quite similar, including the extent of phonon coupling, the temperature dependence and the inhomogeneous broadening.

REFERENCES

1. Stanbury, J. B., Wyngaarden, J. B., and Fredrickson, D. S. (1978) *The Metabolic Basis of Inherited Disease*, McGraw-Hill Book Company, New York.
2. Fujii, M., Hori, H., Miyazaki, G., Morimoto, H., and Yonetani, T. (1993) *J. Biol. Chem. 268*, 15386−15393.
3. Leonard, J. J., Yonetani, T., and Callis, J. B. (1974) *Biochemistry 13*, 1460−1464.
4. Sudhakar, K., Loe, S., Yonetani, T., and Vanderkooi, J. M. (1994) *J. Biol. Chem. 269*, 23095−23101.
5. Peterson-Kennedy, S. E., McGourty, J. L., Kalweit, J. A., and Hoffman, B. A. (1986) *J. Am. Chem. Soc. 108*, 1739−1746.
6. Kuila, D., Baxter, W. W., Natan, M. J., and Hoffman, B. M. (1991) *J. Phys. Chem. 95*, 1−3.
7. McGourty, J. L., Blough, N. V., and Hoffman, B. M. (1983) *J. Am. Chem. Soc. 105*, 4470−4472.
8. Vanderkooi, J. M., Moy, V. T., Maniara, G., Koloczek, H., and Paul, K. G. (1985) *Biochemistry 24*, 7931−7935.
9. Logovinsky, V., Kaposi, A. D., and Vanderkooi, J. M. (1993) *Biochim. Biophys. Acta 1161*, 149−160.
10. Vanderkooi, J. M., Angiolillo, P. J., and Laberge, M. (1997) in *Methods Enzymol. Fluorescence Spectroscopy* (Brand, L., Ed.) pp 71−94, Wiley, New York.
11. Tsuneshige, A., and Yonetani, T. (1994) *Methods Enzymol. 231*, 215−222.
12. Personov, R. I., and Korotaev, O. N. (1969) *Sov. Phys.-Doklady 13*, 1033−1036.
13. Personov, R. I. (1983) in *Spectroscopy and Excitation Dynamics of Condensed Molecular Systems* (Agranovich, V. M., and Hochstrasser, R. M., Eds.) pp 555−619, North-Holland Publishing Co., Amsterdam.
14. Fuenfschilling, J., and Zschokke-Graenacher, I. (1982) *Chem. Phys. Lett. 91*, 122−125.
15. Fidy, J., Paul, K.-G., and Vanderkooi, J. M. (1989) *Biochemistry 28*, 7531−7541.
16. Kaposi, A. D., Logovinsky, V., and Vanderkooi, J. M. (1992) *Proc. Soc. Photo-Opt. Instrum. Eng. 1640*, 792−799.
17. Fermi, G., Perutz, M. F., and Shaanan, B. (1984) *J. Mol. Biol. 175*, 159−174.
18. Nicholls, A., and Honig, B. (1991) *J. Comput. Chem. 12*, 435−445.
19. Anni, H., Vanderkooi, J. M., Sharp, K. A., Yonetani, T., Hopkins, S. C., Herenyi, L., and Fidy, J. (1994) *Biochemistry 33*, 3475−3486.
20. Köhler, M., Gafert, J., Friedrich, J., Vanderkooi, J. M., and Laberge, M. (1996) *Biophys. J. 71*, 77−85.
21. Laberge, M., Vanderkooi, J. M., and Sharp, K. A. (1996) *J. Phys. Chem. 100*, 10793−10801.
22. Gouterman, M. (1978) in *The Porphyrins* (Dolphin, D., Ed.) pp 1−156, Academic Press, New York.
23. Sugita, Y. (1975) *J. Biol. Chem. 250*, 1251−1256.
24. Keilin, D., and Hartree, E. F. (1949) *Nature 164*, 254−259.
25. Reddy, K. S., Angiolillo, P. J., Wright, W. W., Laberge, M., and Vanderkooi, J. M. (1996) *Biochemistry 35*, 12820−12830.
26. Balog, E., Kis-Petik, K., Fidy, J., Kohler, M., and Friedrich, J. (1997) *Biophys. J. 73*, 397−405.
27. Shelnutt, J. A., Cheung, L. D., Chang, R. C. C., Yu, N.-T., and Felton, R. H. (1977) *J. Chem. Phys. 66*, 3387−3398.
28. Gouterman, M. (1973) *Ann. N.Y. Acad. Sci. 206*, 70−83.
29. van der Waals, J. H., van Dorp, W. G., and Schaafsma, T. J. (1979) in *The Porphyrins* (Dolphin, D., Ed.) pp 257−312, Academic Press, New York.
30. Hoffman, B. M. (1975) *J. Am. Chem. Soc. 97*, 1688−1694.
31. Hoffman, B. M., and Ratner, M. A. (1978) *Mol. Phys. 35*, 901−925.
32. Polm, M. W., and Schaafsma, T. J. (1997) *Biophys. J. 72*, 373−382.
33. Angiolillo, P., and Vanderkooi, J. M. (1995) *Biophys. J. 68*, 2505−2518.
34. Galli, C., Wynne, K., LeCours, S. M., Therien, M. J., and Hochstrasser, R. M. (1993) *Chem. Phys. Lett. 206*, 493−499.
35. Kim, B. F., and Bohandy, J. (1977) *J. Mol. Spectrosc. 65*, 90−101.
36. Angiolillo, P. J., Leigh, J. S., Jr., and Vanderkooi, J. M. (1982) *Photochem. Photobiol. 36*, 133−137.
37. Koloczek, H., Fidy, J., and Vanderkooi, J. M. (1987) *J. Chem. Phys. 87*, 4388−4394.
38. Logovinsky, V., Kaposi, A. D., and Vanderkooi, J. M. (1991) *J. Fluoresc. 1*, 79−86.
39. Choi, S., Spiro, T. G., Langry, K. C., Smith, K. M., Budd, D. L., and LaMar, G. N. (1982) *J. Am. Chem. Soc. 104*, 4345−4351.
40. Spiro, T. G., Czernuszewicz, R. S., and Li, X.-Y. (1990) *Coord. Chem. Rev. 100*, 541−571.
41. Hu, S., Morris, I. K., Singh, J. P., Smith, K. M., and Spiro, T. G. (1993) *J. Am. Chem. Soc. 115*, 12446−12458.
42. Ondrias, M. R., Rousseau, D. L., Kitagawa, T., Ikeda-Saito, M., Inubishi, T., and Yonetani, T. (1982) *J. Biol. Chem. 257*, 8766−70.
43. Cowan, J. A., and Gray, H. B. (1989) *Inorg. Chem. 28*, 4554−4556.
44. Ahn, J. S., Kanematsu, Y., Enomoto, M., and Kushida, T. (1993) *Chem. Phys. Lett. 215*, 336−340.
45. Ye, S., Cotton, T., and Kostic, N. M. (1997) *J. Inorg. Biochem. 65*, 219−226.
46. Anni, H., Vanderkooi, J. M., and Mayne, L. (1995) *Biochemistry 34*, 5744−5753.
47. Laberge, M., Sharp, K. A., and Vanderkooi, J. M. (1997) *J. Phys. Chem. 101*, 7364−7367.
48. Goldbeck, R. A., Sagle, L., Kim-Shapiro, D. B., Flores, V., and Kliger, D. S. (1997) *Biochem. Biophys. Res. Commun. 235*, 610−614.
49. Kohler, B. E. (1979) in *Chemical and Biochemical Applications of Lasers, Vol. IV* (Moore, C. B., Ed.) pp 31−53, Academic Press, New York.
50. Iizuka, T., Yamamoto, H., Kotani, M., and Yonetani, T. (1974) *Biochim. Biophys. Acta 371*, 126−139.

BI972786S